blood®
Regular Article

PLATELETS AND THROMBOPOIESIS

The RNA-binding protein SRSF3 has an essential role in megakaryocyte maturation and platelet production

Shen Y. Heazlewood,[1,2,*] Tanveer Ahmad,[1,2,*] Monika Mohenska,[2] Belinda B. Guo,[3] Pradnya Gangatirkar,[4] Emma C. Josefsson,[4,5] Sarah L. Ellis,[6,7] Madara Ratnadiwakara,[2,8,9] Huimin Cao,[1,2] Benjamin Cao,[1,2] Chad K. Heazlewood,[1,2] Brenda Williams,[1,2] Madeline Fulton,[1,2] Jacinta F. White,[1] Mirana Ramialison,[2] Susan K. Nilsson,[1,2,†] and Minna-Liisa Änkö[2,8,9,†]

[1]Biomedical Manufacturing CSIRO, VIC, Australia; [2]Australian Regenerative Medicine Institute, Monash University, VIC, Australia; [3]School of Biomedical Sciences, Pathology and Laboratory Science, University of Western Australia, WA, Australia; [4]Walter and Eliza Hall Institute of Medical Research, VIC, Australia; [5]Department of Medical Biology, The University of Melbourne, VIC, Australia; [6]Peter MacCallum Cancer Centre, and Sir Peter MacCallum Department of Oncology, University of Melbourne, VIC, Australia; [7]Olivia Newton-John Cancer Research Institute, Microscopy Facility and School of Cancer Medicine, La Trobe University, VIC, Australia; [8]Hudson Institute of Medical Research, VIC, Australia; and [9]Department of Molecular and Translational Sciences, Monash University, VIC, Australia

KEY POINTS

- **The RNA binding protein SRSF3 is essential for megakaryocyte maturation and platelet production.**
- **SRSF3-deficient megakaryocytes fail to reprogram their transcriptome during maturation and sort functionally important RNAs into platelets.**

RNA processing is increasingly recognized as a critical control point in the regulation of different hematopoietic lineages including megakaryocytes responsible for the production of platelets. Platelets are anucleate cytoplasts that contain a rich repertoire of RNAs encoding proteins with essential platelet functions derived from the parent megakaryocyte. It is largely unknown how RNA binding proteins contribute to the development and functions of megakaryocytes and platelets. We show that serine-arginine–rich splicing factor 3 (SRSF3) is essential for megakaryocyte maturation and generation of functional platelets. Megakaryocyte-specific deletion of *Srsf3* in mice led to macrothrombocytopenia characterized by megakaryocyte maturation arrest, dramatically reduced platelet counts, and abnormally large functionally compromised platelets. SRSF3 deficient megakaryocytes failed to reprogram their transcriptome during maturation and to load platelets with RNAs required for normal platelet function. SRSF3 depletion led to nuclear accumulation of megakaryocyte mRNAs, demonstrating that SRSF3 deploys similar RNA regulatory mechanisms in megakaryocytes as in other cell types. Our study further suggests that SRSF3 plays a role in sorting cytoplasmic megakaryocyte RNAs into platelets and demonstrates how SRSF3-mediated RNA processing forms a central part of megakaryocyte gene regulation. Understanding SRSF3 functions in megakaryocytes and platelets provides key insights into normal thrombopoiesis and platelet pathologies as SRSF3 RNA targets in megakaryocytes are associated with platelet diseases.

Introduction

Platelets produced by bone marrow megakaryocytes (MKs) are anucleate cytoplasts that play a critical role in normal hemostasis, including vascular integrity, wound healing, and activation of inflammatory and immune responses.[1] MK maturation culminating in platelet release involves polyploidisation through endomitosis, establishment of complex membrane system, cytoplasmic expansion, and generation of platelet granules.[2,3] The complexity of platelet biogenesis is reflected in a range of platelet disorders characterized by abnormal platelet numbers and/or function.[4,5]

Although transcription factors guide lineage decisions,[2,6-11] the discovery of frequent mutations in splicing factor genes such as *SF3B1*, *U2AF1*, and *SRSF2* in myelodysplastic syndrome patients first demonstrated the critical role of posttranscriptional gene regulation during normal hematopoiesis.[12-18] The identification of a widespread intron retention in MK progenitors and in vitro differentiated fetal liver CD41$^+$ MKs suggests that RNA processing plays a central role in tuning MK gene expression.[15] Furthermore, mutations in the RNA binding protein encoding gene *RBM8A* cause thrombocytopenia-absent radius syndrome.[19] Although platelets do not have a nucleus, they contain RNA derived from the parent MK. RNA processing and translation machineries are present in platelets, and alterations in platelet RNA content reflect changes in platelet function.[20-23] Both RNA deposition by MKs and RNA degradation in platelets are regulated, but the factors controlling these processes are largely unknown.[24,25]

RNA binding proteins are required at every step of RNA biogenesis and, thereby, modify the RNA repertoire of cells. Serine-arginine–rich splicing factor 3 (SRSF3) belongs to the family of

SR proteins originally identified as essential pre–messenger RNA (mRNA) splicing factors but their functions now expand to most steps of RNA metabolism.[26-33] SRSF3 regulates distinct sets of RNAs in a cell type–specific manner through multiple RNA processing pathways.[27,32-34] Although some SRSF3 target RNAs are shared between different cells types, many are cell type specific, suggesting distinct SRSF3 functions in each cell type.[27,34] The physiological role of SRSF3 has not been extensively explored because the systemic deletion of *Srsf3* in mice is embryonically lethal.[33,35,36] The hepatocyte-specific deletion of *Srsf3* in mice led to impaired hepatocyte differentiation, whereas in the B-cell lineage it resulted in a reduction of immature and mature B cells.[37,38] At the cellular level, SRSF3 has been shown to regulate cell proliferation, cell cycle progression, and apoptosis in both normal and tumor cells.[33,39-41]

Our phenotypic analysis of the systemic heterozygous *Srsf3* knockout (KO) mice revealed reduced platelet counts, suggesting a role for SRSF3 in platelet production. MK-specific deletion of *Srsf3* (*Pf4-Srsf3*$^{\Delta/\Delta}$) demonstrated a hitherto unknown and critical role for SRSF3 in MK maturation and platelet biogenesis. SRSF3 depletion led to a MK maturation defect and drastically reduced platelet counts. RNA-sequencing of subpopulations of MKs demonstrated that *Pf4-Srsf3*$^{\Delta/\Delta}$ MKs failed to reprogram their transcriptome during maturation. Similar to other cell types, SRSF3 regulated functionally related sets of MK RNAs. SRSF3 acted as mRNA export factor in MKs, its depletion leading to the nuclear accumulation of key MK mRNAs. The RNA content of *Pf4-Srsf3*$^{\Delta/\Delta}$ platelets was abnormal, with ~6000 dysregulated RNAs, suggesting SRSF3 plays a cytoplasmic role in sorting MK RNAs into platelets. The failure of SRSF3-deficient MKs to reprogram their transcriptome and load platelets with RNAs required for normal platelet function demonstrates that SRSF3-mediated RNA processing forms a central part of MK gene regulation and platelet biogenesis.

Methods

Experimental animals

Srsf3 KO mouse model was generated from *Srsf3*$^{tm1a(KOMP)Mbp}$ KO-first embryonic stem cells (UC Davis Mouse Biology Program). C57/Bl6 *Pf4-Srsf3*$^{\Delta/\Delta}$ mouse strain was established by crossing C57Bl/6xCBA *Srsf3*$^{fl/fl}$[33] x C57/Bl6 *Pf4*-Cre[42] and backcrossing to C57/Bl6. The experiments were approved by the Monash University Animal Ethics Committee and performed according to the Australian code for the care and use of animals for scientific purposes by the National Health and Medical Research Council. Male and female mice 6 to 10 weeks of age were used.

Isolation of mouse bone marrow MKs

Iliac crests, femurs and tibiae were collected, cleaned and flushed with 2% fetal bovine serum–phosphate-buffered saline. The flushed cells were filtered (100 μm) and spun 300 g for 5 minutes to harvest the total bone marrow cells. To analyze/isolate bone marrow MKs, lineage-depleted cells were labeled with 10 μM Hoechst 33342, washed, and labeled with AF700-conjugated rat anti-mouse CD41 (Biolegend), hamster anti-mouse CD61-PE (BD Biosciences) or goat anti-mouse Mpl-Biotin (R&D), and SAV-AF647 (Biolegend). The cells were sorted using Influx cell sorter or analyzed using LSRII cell analyzer (Becton Dickinson).

Platelet activation assays

Blood was obtained by cardiac puncture into 0.1vol of Aster-Jandl anticoagulant followed by centrifugation of the supernatant buffy coat. Platelets were washed and platelet counts determined by flow cytometry. Platelets were treated with single agonists adenosine 5′-diphosphate (12.5-50 μM), Convulxin (12.5-50 ng/mL), PAR4-AP (0.125-0.25 mM), or thrombin (0.0625-0.25 U/mL) in the presence of 1 mM $CaCl_2$, and activation of the αIIbβ3 integrin (JON/A) or P-selectin (Emfret Analytics) exposure was assessed by flow cytometry. Diluted whole blood was recalcified, rested, treated with PAR4-AP, and platelet activation was analyzed as above.

Platelet surface receptor analysis

Whole blood collected in ethylenediaminetetraacetic acid was diluted and platelets stained with fluorescently conjugated CD41 (BD Biosciences), GPVI, GPIX, and GP1bα (Emfret Analytics) antibodies. Samples were diluted with phosphate-buffered saline and directly acquired by flow cytometry.

Transmission electron microscopy

Femurs were perfusion fixed with 2.5% glutaraldehyde/2% paraformaldehyde in Sorensen's phosphate buffer and decalcified as above. The fixed femurs and isolated platelets were processed for TEM, sectioned, and imaged.

RNA-sequencing and bioinformatics

CD41$^+$ 8N and ≥ 16N MKs were collected (23 ± 3k and 81 ± 5k, respectively) for RNA isolation (RNeasy Mini kit, Qiagen) followed by library preparation using SMARTer Stranded Total RNA Low Input Sample Prep kit (Clontech) and RNA-sequencing by Illumina HiSeq1500. The reads were aligned with STAR[43] to Ensembl mm10. Differential gene expression analyzed with EdgeR.[44,45]

Platelet RNA was isolated using TriReagent (Sigma-Aldrich). Libraries were prepared using an Ion AmpliSeq Transcriptome Mouse Gene Expression Kit and sequenced on Ion Proton Sequencer (Thermo Fisher).[46] The data were analyzed using Torrent Suite Software v5.6 (Thermo Fisher) and differential gene expression analyzed using DESeq2.[47] Gene ontology enrichment analysis were conducted with DAVID.[48]

RNA immunoprecipitation in MEG-01 cells

MEG-01 megakaryoblasts were transduced with pCCL-SRSF3-GFP or pCCL-GFP vector and GFP$^+$ cells were lysed. The lysate was incubated with GFP-Trap magnetic beads (Chromotek). The beads were washed, RNA isolated using TriReagent (Sigma-Aldrich), and RNA was DNaseI treated (Promega) and reverse transcribed with SuperScript III (Thermo Fisher). Quantitative polymerase chain reaction (qPCR) was performed in QuantStudio6 using Luminaris HiGreen qPCR Master Mix-low ROX (Thermo Fisher) and 0.3 μM primers (supplemental Table 1). The cycle threshold values were calculated and immunoprecipitation normalized to input.

Nucleo-cytoplasmic fractionation of MEG-01 SRSF3 KO cells

MEG-01 cells were transduced with a lentiviral clustered regularly interspaced short palindromic repeats (CRISPR)-associated protein 9 (Cas9)–mCherry reporter vector.[49] Cas9-mCherry$^+$ cells were transduced with a lentiviral vector carrying a single-guide RNA

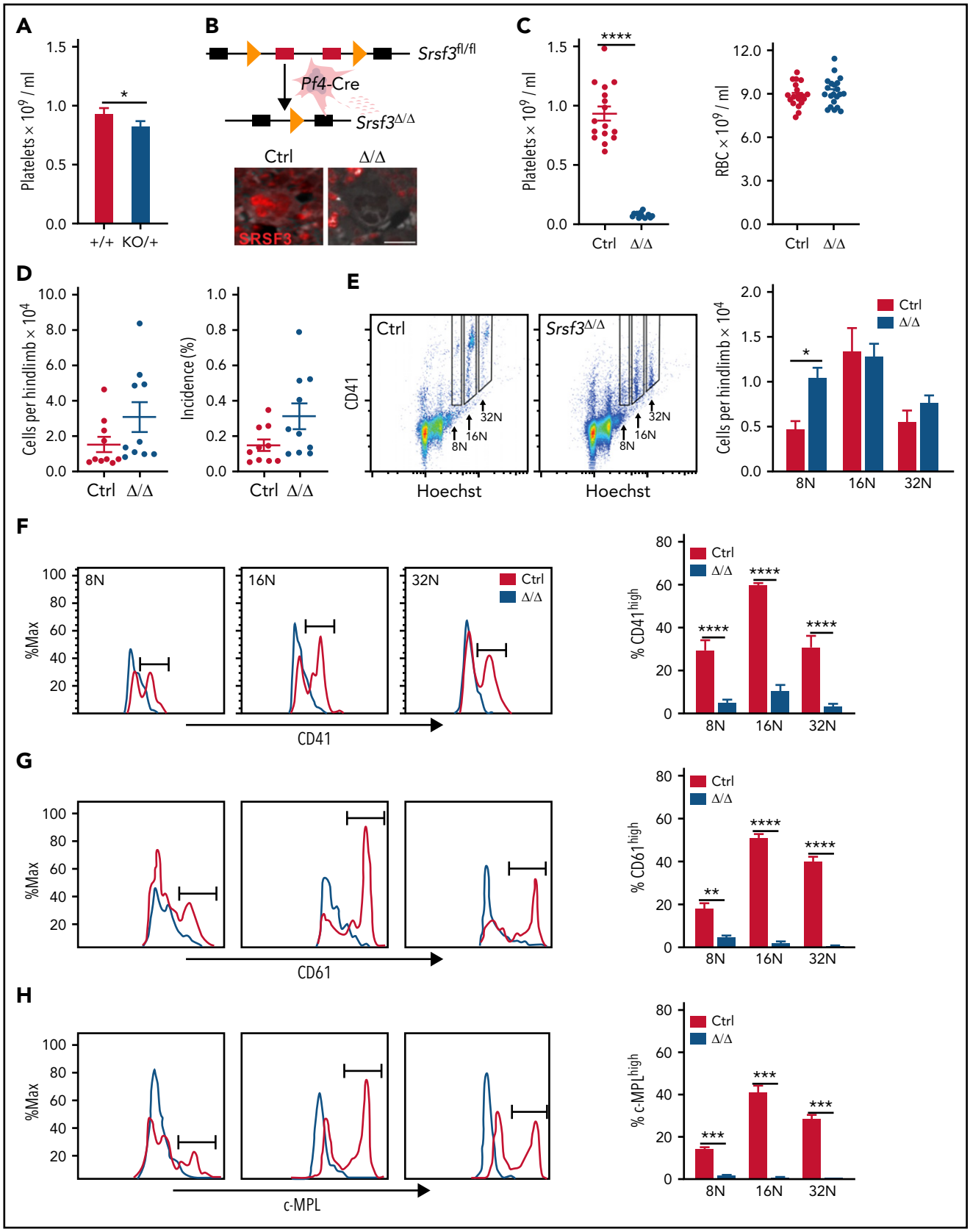

Figure 1. SRSF3 depletion in MKs leads to severe thrombocytopenia without a change in MK numbers. (A) Platelet counts of heterozygous mice (KO/$^{+}$) with a systemic *Srsf3* deletion compared with wild-type mice ($^{+/+}$) (n = 6). (B) Top: Generation of a mouse model where *Srsf3* is deleted in MKs (*Pf4-Srsf3*$^{\Delta/\Delta}$). Bottom: Anti-SRSF3 immunohistochemistry in *Pf4-Srsf3*$^{\Delta/\Delta}$ and control bone marrow sections. (C) Platelet and red blood cell (RBC) counts of control and *Pf4-Srsf3*$^{\Delta/\Delta}$ mice. (D) The total number and incidence of bone marrow MKs in control and *Pf4-Srsf3*$^{\Delta/\Delta}$ mice. (E) The number of MKs of individual ploidy in control and *Pf4-Srsf3*$^{\Delta/\Delta}$ bone marrow. (F) CD41, (G) CD61, and (H) c-MPL cell surface receptor expression of control and *Pf4-Srsf3*$^{\Delta/\Delta}$ MKs. A histogram of a representative mouse is shown (n = 4). The proportion of events in the gate marked in the histogram (CD41/CD61/c-MPL^{high}) is quantified on the right. The data are presented as mean plus or minus standard error of the mean (SEM). Two-tailed unpaired Student *t* test in panels A and C through D; 2-way analysis of variance (ANOVA) in panels E through H. ****$P \leq .0001$; ***$P \leq .001$; **$P \leq .01$; *$P \leq .05$. Δ/Δ, *Pf4-Srsf3*$^{\Delta/\Delta}$ mice; Ctrl, control.

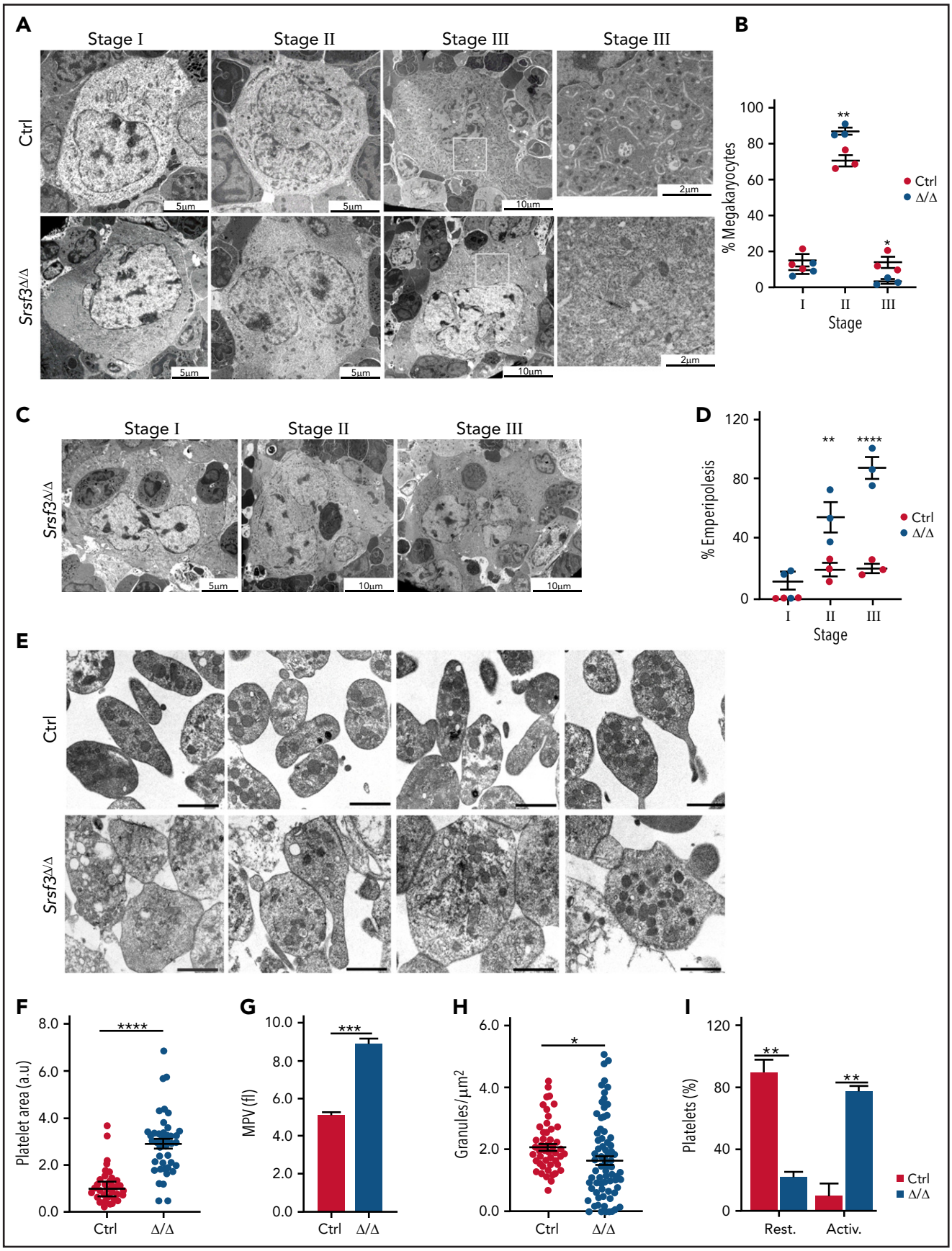

Figure 2. SRSF3 depletion leads to MK maturation arrest and macrothrombocytopenia. (A) Representative TEM images depicting the ultrastructure of control and *Pf4-Srsf3*$^{\Delta/\Delta}$ MKs at stage I, II, and III of maturation. Scale bars represent 5, 10, and 10 μm, respectively. On the right, a higher magnification of the boxed areas in stage

targeting *SRSF3* or scrambled control (h*SRSF3*[gRNA#326] or Scramble[gRNA#1], Vector Builder). Forty-eight hours post-transduction, the cells were harvested and total, nuclear, and cytoplasmic fractions isolated.[33] RNA from each fraction was used for reverse transcription (RT)-qPCR performed as above. 18S ribosomal RNA and U6 small nuclear RNA were used to determine the purity of the fractions (Applied Biosystems TaqMan MicroRNA Reverse Transcription Kit, [Thermo Fisher Scientific], SensiFAST Probe Hi-ROX Kit [Bioline] and U6 probe [Assay ID 001973, Thermo Fisher]). Caspase3/7 activity was measured from transduced cells with the Caspase Glo-3/7 assay (Promega).

Results

SRSF3 ablation in MKs results in severe thrombocytopenia without a change in MK numbers

Systemic depletion of *Srsf3* is lethal at the morula stage,[35] hampering the investigation of SRSF3 functions in adult cell types. Although heterozygous *Srsf3* KO mice were born in expected numbers, ~50% died before weaning (supplemental Figure 1A).[35] The surviving *Srsf3*$^{KO/+}$ mice were anatomically and morphologically normal and had close to normal levels of SRSF3 protein and mRNA in the examined tissues, demonstrating that the autoregulatory feedback control observed in cell lines also operated in mouse tissues to maintain SRSF3 levels (supplemental Figure 1B-C).[32,50] However, *Srsf3*$^{KO/+}$ mice presented reduced platelet counts without a decrease in bone marrow MK numbers (Figure 1A; supplemental Figure 1D-E). To specifically investigate SRSF3 in MKs and platelets, we generated a MK-specific *Srsf3* KO mouse model (hereafter *Pf4-Srsf3*$^{\Delta/\Delta}$ or Δ/Δ) (Figure 1B).[33,42] Immunohistochemistry of bone marrow sections indicated successful SRSF3 ablation in MKs (Figure 1B). The *Pf4-Srsf3*$^{\Delta/\Delta}$ mice were viable and fertile with the expected number of offspring (supplemental Figure 1A). The mice had >90% reduction in their peripheral blood platelet counts, whereas red blood cells originating from the same progenitors were not affected, and white blood cells were slightly increased (Figure 1C; supplemental Figure 1F). The total number and incidence of bone marrow MKs were unchanged in *Pf4-Srsf3*$^{\Delta/\Delta}$ mice (Figure 1D), whereas the total number and incidence of myeloid cells was increased, B cells decreased, and T cells unchanged (supplemental Figure 1G-H).

MKs are marked by the expression of cell surface glycoproteins including CD41 (integrin αIIb), CD61 (integrin β3), and c-MPL, and MK ploidy correlates with their maturation stage.[2,51-54] Flow cytometric analysis of *Pf4-Srsf3*$^{\Delta/\Delta}$ MKs showed no reduction in MKs within individual ploidies (Figure 1E; supplemental Figure 1I), suggesting that endomitosis was not affected. *Srsf3*-null MKs expressed CD41, CD61, and c-MPL at a lower level than the control MKs across ploidies as demonstrated by the significant reduction in the high intensity population (CD41/CD61/c-MPL^{high}) of the bimodal distributions across ploidies (Figure 1F-H). Immunohistochemistry of bone marrow sections supported these findings (supplemental Figure 1J).

SRSF3 depletion leads to MK maturation arrest and macrothrombocytopenia

We next assessed MK maturation in *Pf4-Srsf3*$^{\Delta/\Delta}$ bone marrow using transmission electron microscopy (TEM). MKs can be divided into 3 distinct maturation stages based on morphological features such as the presence of α-granules, dense granules, and demarcation membrane system.[55] Analysis of control and *Pf4-Srsf3*$^{\Delta/\Delta}$ bone marrow sections demonstrated a MK maturation arrest following *Srsf3* ablation (Figure 2A-B; supplemental Figure 2A-C). The stage III MKs characterized by a multilobulated nucleus, well-developed demarcation membrane system, and abundant platelet granules were missing (Figure 2A-B; supplemental Figure 2C), whereas the number of stage I megakaryoblasts (1-50 μm in diameter, a kidney-shaped nucleus, and high nuclear-to-cytoplasm ratio) was unchanged (Figure 2A-B; supplemental Figure 2B), and the stage II MKs (20-80 μm in diameter with an irregularly shaped nucleus) were increased in numbers (Figure 2A-B; supplemental Figure 2A). The TEM analysis also revealed substantial emperipolesis (engulfment of intact cells) in *Srsf3*-null MKs, particularly at stage II and III (Figure 2C-D).

Ultrastructural analysis of platelets demonstrated that the remaining 5% to 10% of platelets in *Pf4-Srsf3*$^{\Delta/\Delta}$ mice were approximately twofold larger in size than controls (Figure 2E-F; supplemental Figure 2D), supported by increased mean platelet volume and flow cytometric analysis (Figure 2G; supplemental Figure 2E). Mature platelets contain abundant secretory granules including dense granules, α-granules, and lysosomes that arise from the MK trans-Golgi network.[56] Quantification of granules per platelet surface area showed a significant reduction in the granule density following SRSF3 depletion (Figure 2H). The *Srsf3*-null platelets also contained dilated vacuoles that previous studies have proposed to represent empty α-granules (Figure 2E).[57] Morphological features such as shape and granule localization can be indicative of platelet activation status. Resting platelets are typically discoid in shape, whereas activated platelets are rounded with centralized granules and filopodia. Based on these morphological criteria, the majority of *Srsf3*-null platelets appeared activated compared with the controls that appeared largely resting (Figure 2I), in agreement with the reduced granularity of *Srsf3*-null platelets (Figure 2H). Taken together, the ultrastructural analysis of MKs and platelets revealed that following a maturation arrest, SRSF3-deficient MKs released abnormally large platelets presenting morphological features typical for activated platelets.

Srsf3-null platelets are primed for activation

Unlike MKs, CD41 cell surface expression was not altered in *Srsf3*-null platelets, suggesting that the remaining CD41 receptor pool

Figure 2 (continued) III MKs. Scale bars represent μm. (B) Quantification of control and *Pf4-Srsf3*$^{\Delta/\Delta}$ MKs at each stage of maturation. (C) Representative TEM images of *Pf4-Srsf3*$^{\Delta/\Delta}$ MKs at stage I, II, and III of maturation displaying emperipolesis. Scale bars represent 5, 10, and 10 μm, respectively. (D) Quantification of the fraction of *Pf4-Srsf3*$^{\Delta/\Delta}$ MKs at each maturation stage displaying emperipolesis. (E) Representative TEM images of control and *Pf4-Srsf3*$^{\Delta/\Delta}$ platelets. Scale bars are 1 μm. (F) Quantification of control and *Pf4-Srsf3*$^{\Delta/\Delta}$ platelet area. (G) Mean platelet volume of control and *Pf4-Srsf3*$^{\Delta/\Delta}$ platelets. (H) Quantification of the number of granules in control and *Pf4-Srsf3*$^{\Delta/\Delta}$ platelets. (I) Quantification of the fraction of resting and activated control and *Pf4-Srsf3*$^{\Delta/\Delta}$ platelets. Platelets with filopodia, rounded shape, and/or centralised granules were classified as activated. The data are presented as mean plus or minus SEM. Two-way ANOVA in panels B and D and 2-tailed unpaired Student *t* test in panels F through I. ****$P \leq .0001$; ***$P \leq .001$; **$P \leq .01$; *$P \leq .05$. Activ, activated; rest, resting.

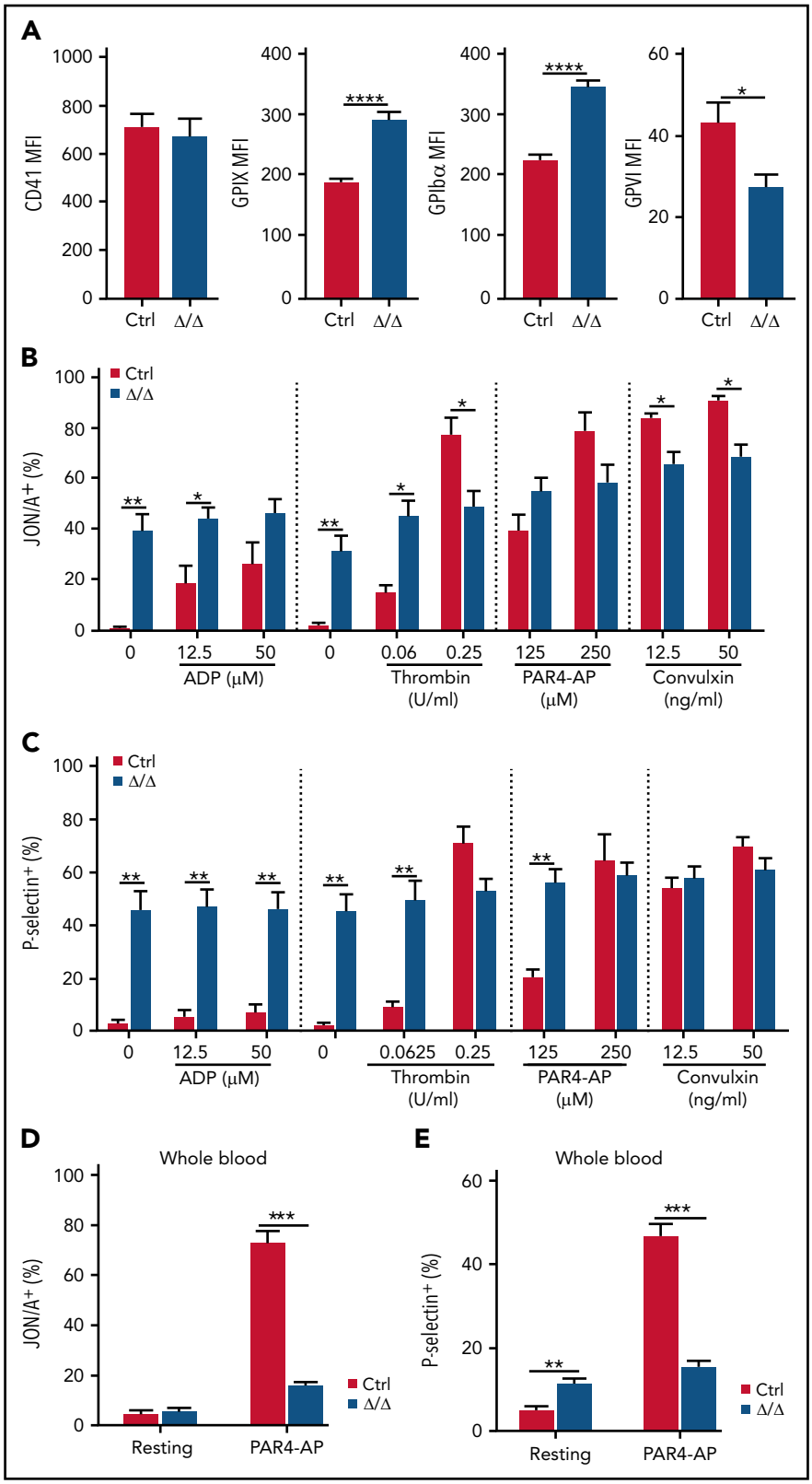

Figure 3. *Srsf3*-null platelets are preactivated. (A) The mean fluorescence intensity (MFI) of CD41, GPIX, GPIbα, and GPVI cell surface receptors in control and *Pf4-Srsf3*$^{\Delta/\Delta}$ platelets assessed in diluted whole blood. (B-C) The expression of activated Integrin-αIIb-β3 receptor (JON/A) and P-selectin on the surface of washed control and *Pf4-Srsf3*$^{\Delta/\Delta}$ platelets following agonist stimulation. (D-E) The expression of activated Integrin-αIIb-β3 receptor (JON/A) and P-selectin on the surface of control and *Pf4-Srsf3*$^{\Delta/\Delta}$ platelets from diluted whole blood. The data are presented as mean plus or minus SEM. Two-tailed unpaired Student *t* test. ***$P \leq .001$; **$P \leq .01$; *$P \leq .05$.

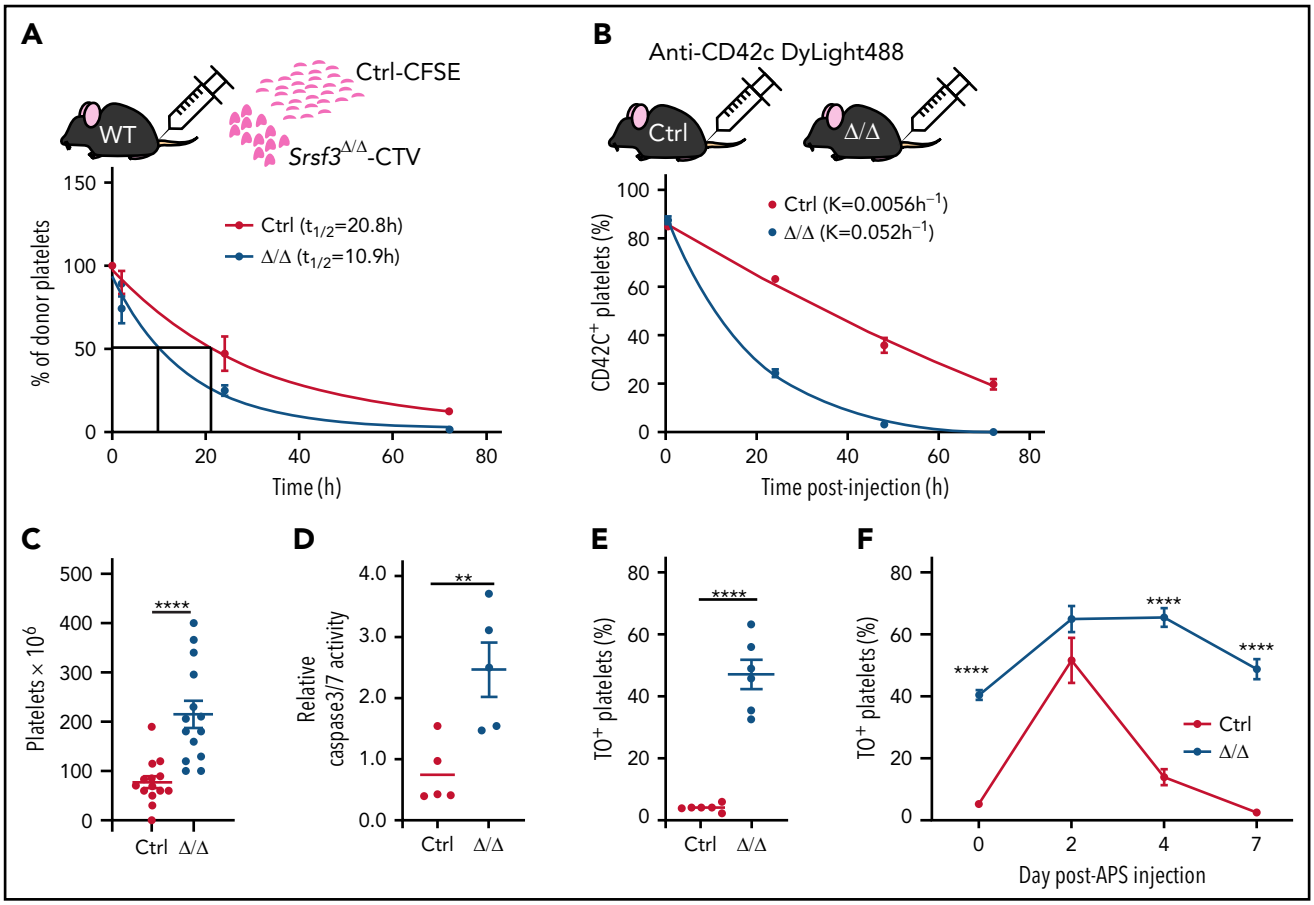

Figure 4. *Srsf3*-null platelets are rapidly cleared from circulation. (A) The half-life of control and *Pf4-Srsf3*$^{\Delta/\Delta}$ platelets as measured by the transplantation of CFSE- and CTV-labeled platelets, respectively, into wild-type mice. The data were fitted to a 1-phase exponential decay curve, and the half-life ($t_{1/2}$) for control (R^2 = 0.932) and *Srsf3*$^{\Delta/\Delta}$ (R^2 = 0.937) platelets is depicted in the inset. (B) The clearance rate of control and *Pf4-Srsf3*$^{\Delta/\Delta}$ platelets as measured by in vivo labeling of platelets by anti-CD42c DyLight488 antibody in control and *Pf4-Srsf3*$^{\Delta/\Delta}$ mice. The data were fitted to a 1-phase exponential decay curve, and the rate constant K for control (R^2 = 0.991) and *Srsf3*$^{\Delta/\Delta}$ (R^2 = 0.996) platelets is depicted in the inset. (C) The number of platelets in the spleen of control and *Pf4-Srsf3*$^{\Delta/\Delta}$ mice. (D) Relative Caspase 3/7 activity in control and *Pf4-Srsf3*$^{\Delta/\Delta}$ platelets. (E) Fraction of reticulated TO$^+$ platelets in control and *Pf4-Srsf3*$^{\Delta/\Delta}$ mice in the steady-state. (F) The fraction of TO$^+$ platelets in control and *Pf4-Srsf3*$^{\Delta/\Delta}$ mice following antiplatelet serum (APS) administration. The data are presented as mean plus or minus SEM. Two-tailed unpaired Student *t* test in panels C through E; 2-way ANOVA in panel F. ****$P \leq .0001$; **$P \leq .01$. CFSE, carboxyfluorescein succinimidyl ester; CTV, CellTrace™ Violet.

in the MKs, albeit reduced, may be sufficient for the small number of *Srsf3*-null platelets produced. GPIbα (CD42b) and GPIX (CD42a) levels were increased, potentially due to the larger size (Figure 3A). In contrast, GPVI (GP6) expression was reduced in *Srsf3*-null platelets (Figure 3A; supplemental Figure 3A-B). To assess the functionality of the *Srsf3*-null platelets, we purified control and *Pf4-Srsf3*$^{\Delta/\Delta}$ platelets, stimulated them in vitro with platelet agonists, and measured platelet degranulation by cell surface P-selectin and integrin receptor conformational change by JON/A-detecting activated Integrin-αIIb-β3 receptor. Control platelets displayed a dose-dependent response to agonist stimulation, whereas the *Srsf3*-null platelets were close to maximally preactivated in vitro without agonist stimulation (Figure 3B-C; supplemental Figure 3C). To exclude that platelet purification affected the degranulation process, we assessed platelet activation status in diluted whole blood. Untreated *Pf4-Srsf3*$^{\Delta/\Delta}$ platelets were preactivated in whole blood when measured by P-selectin but not JON/A (Figure 3D-E; supplemental Figure 3D), suggesting that integrin receptor conformational change (JON/A) was less affected in vivo compared with P-selectin surface exposure involving degranulation. The magnitude of *Srsf3*-null platelet response to agonist stimulation in whole blood was significantly reduced compared with control platelets when measured by both P-selectin and JON/A (Figure 3D-E; supplemental Figure 3D); thus, platelet function was compromised, although some activation potential was retained.

SRSF3 deficient platelets are rapidly cleared from circulation

Reduced platelet counts and abnormally large platelets are a characteristic of human macrothrombocytopenias, where large platelets are released and rapidly consumed or destroyed in the spleen.[58,59] We assessed platelet clearance rate by transfusing isolated fluorescently labeled *Srsf3*-null and wild-type platelets into wild-type mice. The half-lives of *Srsf3*-null–CellTrace™ Violet and wild-type–carboxyfluorescein succinimidyl ester platelets were 10.9 hours and 20.8 hours, respectively (Figure 4A), confirming that *Pf4-Srsf3*$^{\Delta/\Delta}$ platelets are functionally different to wild-type platelets. We also labeled circulating platelets in vivo by injecting anti-CD42c-Dylight-488 antibody into control and *Pf4-Srsf3*$^{\Delta/\Delta}$ mice and assessed platelet retention postinjection. The *Srsf3*-null platelets were cleared 9.3 times faster than control platelets in vivo (Figure 4B).

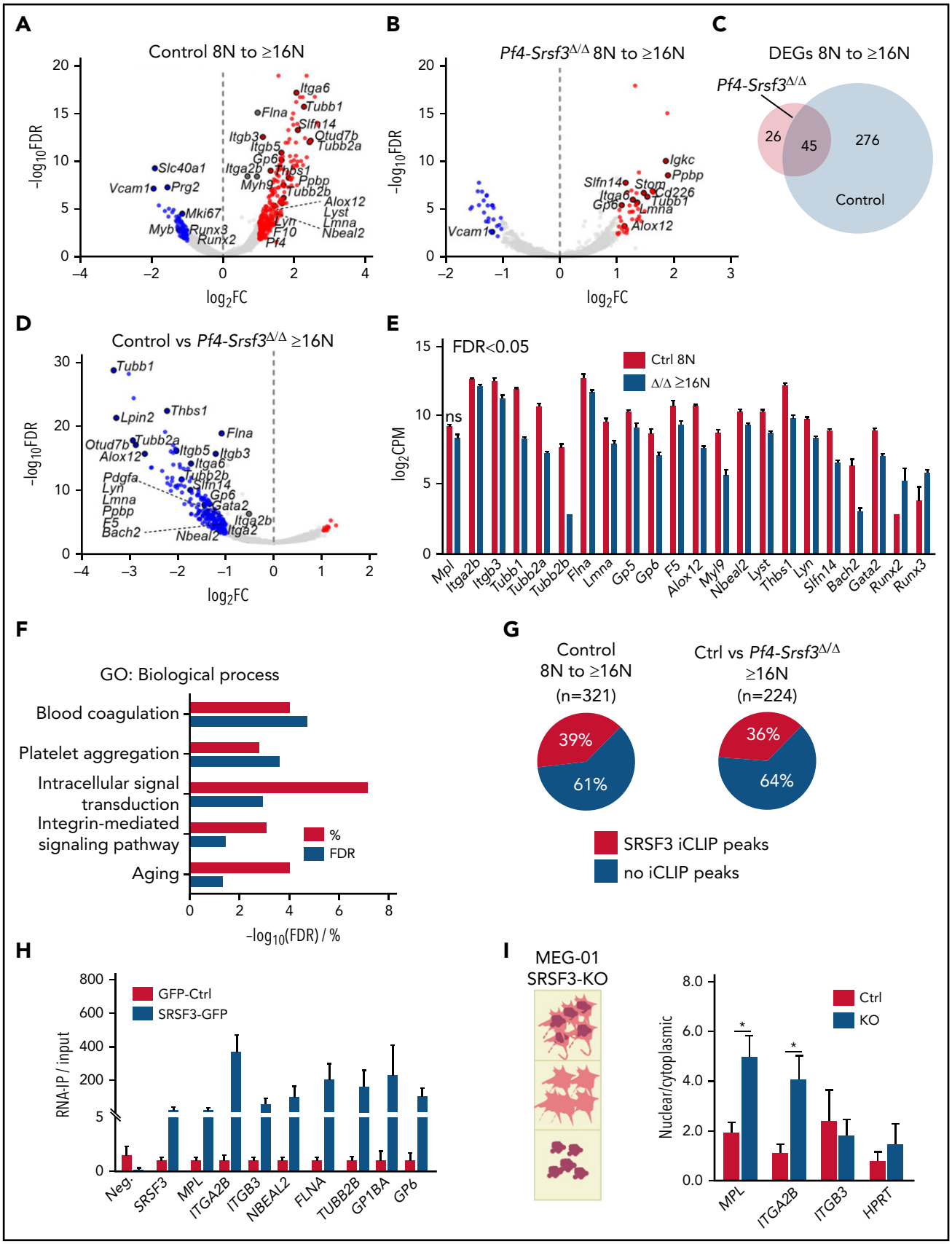

Figure 5. The RNA repertoire of *Srsf3*-null MKs reflects the failure in activating the maturation program. (A) Volcano plots depicting differentially expressed genes (DEGs) between control 8N and ≥16N MKs. The data points marked with blue and red denote significantly down- and upregulated genes (FDR <0.05 and FC >2), respectively. (B) Volcano plots depicting DEGs between *Pf4-Srsf3*$^{\Delta/\Delta}$ 8N and ≥16N MKs as in panel A. (C) Venn diagram comparing DEGs in control and

Pf4-Srsf3$^{\Delta/\Delta}$ mice displayed splenomegaly and increased spleen platelet content (Figure 4C; supplemental Figure 4A), suggesting that the large platelets may be targeted for destruction in the spleen. Accordingly, the analysis of Caspase 3/7 activity demonstrated a significant increase in apoptotic platelets in *Pf4-Srsf3*$^{\Delta/\Delta}$ mice (Figure 4D). This was supported by an increase in phosphatidylserine exposure measured by AnnexinV binding (supplemental Figure 4B). Phosphatidylserine exposure can also be indicative of procoagulation pathway activation, although we did not observe platelet ballooning by TEM. Thiazole orange (TO) labeling of newly generated reticulated platelets[60] showed that the proportion of nascent platelets was increased in *Pf4-Srsf3*$^{\Delta/\Delta}$ mice in steady-state (<5% in control vs >40% in *Pf4-Srsf3*$^{\Delta/\Delta}$), indicative of constant platelet production (Figure 4E). To further assess the dynamics of platelet production capacity and destruction, APS was used to transiently remove circulating platelets. Following APS administration, the number of control platelets plummeted within 24 hours and returned to baseline within 4 days, followed by a further increase above steady-state levels before reaching homeostasis (supplemental Figure 4C). *Srsf3*-null platelet counts rapidly decreased within 24 hours following APS administration and recovered back to steady-state levels by day 4 but never peaked above steady-state levels, unlike in controls (supplemental Figure 4D). The proportion of nascent TO^{+} platelets in *Pf4-Srsf3*$^{\Delta/\Delta}$ mice was pronounced following the APS challenge (Figure 4F). Taken together, the rapid clearance of platelets in *Pf4-Srsf3*$^{\Delta/\Delta}$ mice reflected both an increased platelet demand due to reduced platelet counts and a rapid destruction of the abnormal platelets. The flattened APS response demonstrated a limited platelet production following physiological challenge.

SRSF3 is critical for a transcriptome shift during MK maturation

Given SRSF3′s role in RNA biogenesis, we next investigated how SRSF3 depletion affects the MK RNA repertoire during maturation. Low- (8N) and high-ploidy (≥16N) control and *Srsf3*-null MKs were subjected to RNA-sequencing (supplemental Figure 5A-B). From 8N to higher ploidies, the control MKs underwent a significant transcriptome shift characterized by an upregulation of RNAs encoding MK- and platelet-specific functions (Figure 5A; supplemental Figure 5C; Table 1; supplemental Table 2). This shift was largely absent in *Srsf3*-null MKs (Table 1; Figure 5B-C), reflecting their maturation defect. SRSF3 depletion led to broader gene expression changes in the high-ploidy than the low-ploidy transcriptome (Table 1; Figure 5D; supplemental Figure 5D; supplemental Table 2), further emphasizing the failure of *Srsf3*-null MKs to switch on the mature MK gene expression program. The majority of the dysregulated genes were intron-containing and encoded more than 1 transcript isoform (supplemental Table 2). SRSF3 depletion affected functionally related genes encoding proteins of the cytoskeleton, surface glycoproteins and their receptors, and transcription factors essential for MK maturation (Figure 5E-F; supplemental Figure 5E-F). The human homologs of dysregulated genes such as *Nbeal2* and *Slfn14* are associated with human platelet diseases, and their loss-of-function mutations display phenotypic similarities with the loss of SRSF3 in MKs (Figure 5E-F; Table 2).[61-63]

In vivo MKs are not amenable to UV crosslinking and immunoprecipitation (CLIP) due to their low numbers and unavailability of immunopurification-grade SRSF3 antibodies.[33] To identify direct SRSF3 RNA targets in MKs, we compared the RNA-sequencing data with our previous CLIP data from mouse pluripotent stem cells.[33] Although MKs express many lineage specific genes, one-third of RNAs differently expressed during MK maturation and following SRSF3 depletion were identified as direct SRSF3 RNA targets in mouse pluripotent cells (Figure 5G), suggesting that alterations in MK RNA repertoire were directly mediated by SRSF3. To study MK-specific RNAs, we established a human MEG-01 megakaryoblast cell line expressing a GFP-tagged SRSF3 or GFP as a control (supplemental Figure 5G).[28,33] RNA immunoprecipitation followed by RT-qPCR analysis demonstrated that SRSF3 directly bound to RNAs encoding hallmark proteins in MKs and platelets such as *MPL*, *ITGA2B* (encoding CD41), and *ITGB3* (CD61) (Figure 5H). SRSF3 is a known mRNA export adaptor facilitating the nucleo-cytoplasmic export of selected mRNAs.[28,64,65] CD41, CD61, and c-MPL protein levels on the cell surface were greatly reduced (Figure 1F-H), but their corresponding mRNA levels were affected to much lesser extent in *Srsf3*-null MKs (Figure 5E), suggestive of an mRNA export defect. We analyzed the subcellular distribution of *MPL*, *ITGA2B*, and *ITGB3* mRNAs in MEG-01 cells where *SRSF3* was deleted by CRISPR/Cas9-mediated gene editing (supplemental Figure 5H). SRSF3-depleted MEG-01 cells were separated into total, nuclear, and cytoplasmic fractions, and mRNA levels were assessed in the fractions (Figure 5I; supplemental Figure 5I). Similar to bone marrow MKs, the total *MPL*, *ITGA2B*, and *ITGB3* mRNA levels were minimally affected, and there was no change in cell numbers or increase in apoptosis following SRSF3 depletion in MEG-01 cells (supplemental Figure 5J-L). However, *MPL* and *ITGA2B* mRNAs significantly accumulated in the nucleus in SRSF3-depleted MEG-01 cells with a corresponding decrease in the cytoplasm (Figure 5I; supplemental Figure 5M). This mechanistically may explain why a small change in *Mpl* and *Itga2b* total mRNA levels could lead to a large reduction in their respective protein levels. Taken together, these data demonstrate that SRSF3 regulates functionally related sets of MK RNAs through RNA regulatory mechanisms it deploys in other cell types, suggesting a conserved and critical role for SRSF3 in RNA regulation during MK maturation.

Figure 5 (continued) *Pf4-Srsf3*$^{\Delta/\Delta}$ MKs upon 8N to ≥16N transition. (D) Volcano plot depicting DEGs between control and *Pf4-Srsf3*$^{\Delta/\Delta}$ ≥16N MKs as in panel A. (E) Expression of genes encoding proteins central for MK structure and function in control and *Pf4-Srsf3*$^{\Delta/\Delta}$ ≥6N MKs. FDR <0.05 unless otherwise noted. (F) Significantly enriched GO terms (Biological Process) among DEGs between control and *Pf4-Srsf3*$^{\Delta/\Delta}$ ≥16N MKs (FDR <0.05, FC >2). The x-axis depicts percent genes and -$\log_{10}$ (FDR) of each category. (G) Percentage of RNAs with SRSF3 RNA binding sites (iCLIP peaks) as identified in mouse pluripotent stem cells[33] within RNAs induced during MK maturation (left) or differentially expressed between control and *Pf4-Srsf3*$^{\Delta/\Delta}$ ≥16N MKs (right). (H) RNA immunoprecipitation (IP) using anti-GFP antibody in MEG-01 megakaryoblast cell lines expressing SRSF3-GFP or only GFP. The y-axis denotes the enrichment of SRSF3 RNA binding over input as measured by RT-qPCR (n = 3). Neg. is a nontarget and *SRSF3* a known-target control to demonstrate the specificity of the RNA-IP. (I) Quantification of RNAs in the nuclear and cytoplasmic fractions of MEG-01 cells following *SRSF3* deletion by CRISPR/Cas9 gene editing. The data are presented as a ratio of nuclear and cytoplasmic mRNA abundance (n = 3). *$P \leq .05$. Ctrl, MEG-01 cells targeted with scrambled control guide RNA; FC, fold change; FDR, false discovery rate; KO, MEG-01 cells targeted with SRSF3 guide RNA; ns, not significant.

Table 1. Summary of DEGs following SRSF3 depletion in MK and platelets. Abs(Log_2FC) = 1 and FDR <0.05

	Total	Upregulated	Downregulated
Ctrl: 8N vs ≥16N	321	258	63
Δ/Δ: 8N vs ≥16N	71	46	25
8N: Ctrl vs Δ/Δ	42	11	31
≥16N: Ctrl vs Δ/Δ	224	11	213
Platelets: Ctrl vs Δ/Δ	5827	3120	2707

The RNA repertoire of Srsf3-null platelets is drastically altered

Although platelets are anucleate, they contain a broad repertoire of RNAs.[23] Platelet RNAs are largely deposited by MKs that also transfer cellular machineries such as ribosomes and RNA degradation machinery into platelets.[20,22,25,66-68] The platelet RNA repertoire reflects platelet-specific functions with recent evidence of selective loading of distinct MK RNAs into platelets.[24,69] In accordance with the larger fraction of TO^+ platelets in *Pf4-Srsf3*$^{\Delta/\Delta}$ mice, we detected ~20 times more RNA per *Srsf3*-null platelet compared with control but no difference in the respective MK RNA content (Figure 6A). RNA-sequencing of purified control and *Srsf3*-null platelets demonstrated that SRSF3 depletion in MKs led to a drastically altered platelet RNA profile (Table 1; Figure 6B; supplemental Figure 6A; supplemental Table 2). Functionally important RNAs such as those

Table 2. DEGs in ≥16N *Srsf3*-null MKs associated with human platelet disorders and key MK functions

DEG	logFC	FDR	Protein function	Human disease manifestation
Tubb1	−3.32	1.6×10^{-27}	Part of microtubules driving proplatelet elongation	(Macro)thrombocytopenia
Tubb2a	−2.93	1.3×10^{-16}		
Tubb2b	−1.91	1.5×10^{-10}		
Lyn	−1.20	2.1×10^{-3}	*Lyn*$^{-/-}$ mice thrombocytopenic	Thrombocytopenia
Lyst	−1.39	2.0×10^{-4}	Platelet secretion	Chediak-Higashi syndrome
Alox12	−2.67	1.4×10^{-14}	Arachidonate 12-lipoxygenase predominantly found in platelets	Potentially thrombocytopenia
P2ry12	−1.72	3.3×10^{-5}	Platelet aggregation	Impaired platelet aggregation
Slfn14	−1.73	6.5×10^{-9}	Unknown	Thrombocytopenia and platelet release defects; enlarged platelets
Nbeal2	−0.90	5.0×10^{-2}	α-granule formation and secretion	Gray platelet syndrome (GPS)
Rasgrp2	−1.03	1.0×10^{-2}	Platelet inside out signaling	Reduced ability to perform integrin inside-out signaling
Itga2b	−0.52	3.3×10^{-5}	Essential receptors for MK and PLT integrin signaling	*ITGA2B/ITGB3*-related thrombocytopenia
Itgb3	−1.21	1.4×10^{-14}		
Itgb5	−2.02	5.2×10^{-15}		
Gp6	−1.33	9.7×10^{-7}	Collagen receptor	Impaired platelet aggregation
F5	−1.29	8.1×10^{-5}	Clotting factor	Factor V Leiden blood clotting disorder
Vwf	−0.97	9.15×10^{-13}	Platelet aggregation	Platelet-type or type 2B von Willebrand disease
Myh9	−0.71	5.0×10^{-5}	Cell motility and structure	eg, *MYH9*-RD inherited thrombocytopenia
Flna	−1.09	1.1×10^{-17}	Integrin-receptor anchoring protein	*FLNA*-related thrombocytopenia

Based on Balduini and Savoia[59] and Fisher and Di Paola.[70]

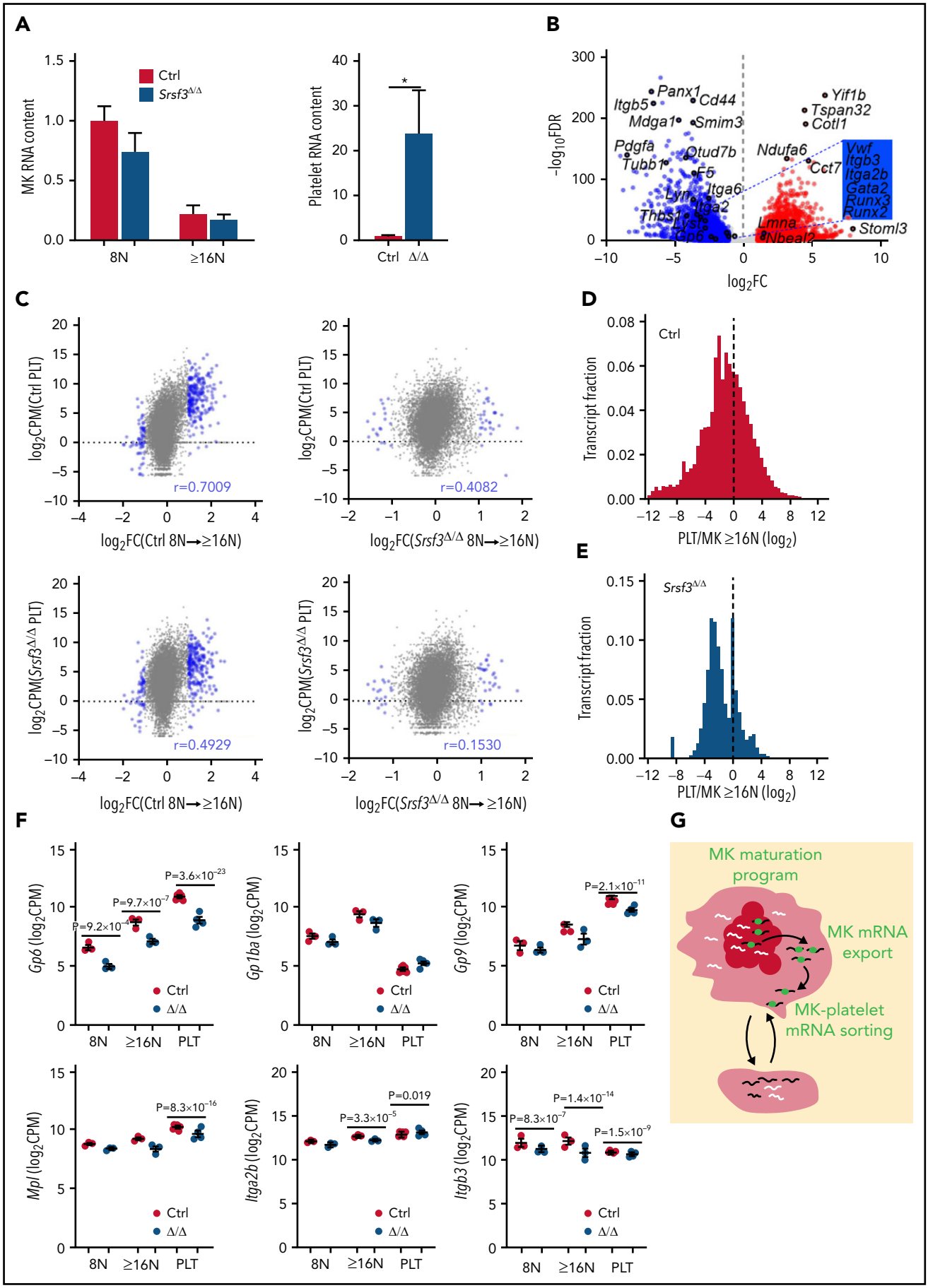

Figure 6. SRSF3 depletion in MKs results in aberrant loading of RNA into platelets. (A) Relative RNA content of control and *Pf4-Srsf3*$^{\Delta/\Delta}$ MKs and platelets (n = 3-6). (B) Volcano plot depicting differential RNA repertoire between control and *Pf4-Srsf3*$^{\Delta/\Delta}$ platelets. The data points marked with blue were significantly less

encoding tubulins, integrin receptors, and their ligands and signaling molecules were either downregulated or absent in the *Srsf3*-null platelets (Figure 6B; supplemental Figure 6B; supplemental Table 2). Instead, a large pool of RNAs not detected in control platelets was present in *Srsf3*-null platelets. We detected 17/40 of the previously listed nonubiquitous top mouse platelet RNAs within the 40 most highly expressed RNAs in the control platelets, whereas only 8/40 in the *Srsf3*-null platelets (supplemental Table 3).[22] The control platelet RNA repertoire, but not the *Srsf3*-null platelet RNA pool, was enriched with RNAs induced during MK maturation (Figure 6C). If platelet RNA content directly reflected MK RNA content, PLT/MK enrichment distribution would be centered at 0. However, similar to previous findings, the platelet/MK RNA abundance ratio was left-skewed in the control, indicating an enrichment of distinct MK RNAs in platelets (Figure 6D; median −1.056 and mean −1.157; supplemental Figure 6C-D).[25] In *Pf4-Srsf3*$^{\Delta/\Delta}$, the platelet/MK RNA ratio distribution was narrow, bimodal, and further left-shifted (Figure 6E; median −1.900 and mean −1.556; supplemental Figure 6D). The abnormal platelet RNA content was also evident at the level of specific RNAs (Figure 6F; supplemental Figure 6E). Because SRSF3 protein levels in platelets were low (supplemental Figure 6F), the discordance of *Pf4-Srsf3*$^{\Delta/\Delta}$ MK and platelet RNAs likely reflected a failure to restrict or facilitate the deposition of distinct MK RNAs into platelets during MK maturation and platelet release (Figure 6G), the abnormal RNA content contributing to the functional defects observed in *Pf4-Srsf3*$^{\Delta/\Delta}$ platelets.

Discussion

Here, we identify the RNA binding protein SRSF3 as a previously unknown regulator of MK maturation and platelet biogenesis. Firstly, we demonstrate that SRSF3 deletion in MKs leads to severely reduced platelet counts without affecting MK numbers. In the absence of SRSF3, MKs fail to reprogram their transcriptome and develop to MKs capable of efficient platelet production. SRSF3 controls MK maturation through RNA regulatory mechanisms that it deploys in other cell types including the regulation of the nucleo-cytoplasmic mRNA export. Secondly, the *Srsf3*-null platelets display multiple deficits including abnormally large size, reduced granule content, and activation in the absence of agonists. The RNA repertoire of *Srsf3*-null platelets is drastically altered, suggesting SRSF3 plays a role in sorting of MK RNAs for deposition into platelets. RNAs encoding proteins with roles in platelet activation were missing in *Srsf3*-null platelets, indicating a functional link between selective RNA loading and platelet function.

The identification of splicing factor mutations as a major cause of myelodysplastic syndrome first proposed that blood lineages may be particularly vulnerable to RNA processing defects.[12-18] RNA expression profiles play a key role in understanding megakaryopoiesis and platelet function.[70,71] To better understand how thrombopoiesis is controlled, it is important to form a comprehensive picture of RNA signatures associated with MK maturation steps and the relationship between MK and platelet RNA. Published RNA-sequencing studies are largely limited to in vitro cultured murine fetal liver MKs, in vitro differentiated human MKs, and cell line models.[15,70] Our native low- and high-ploidy bone marrow MK and matching platelet RNA-sequencing data sets revealing a large transcriptome shift from 8N to higher ploidies (Figure 5A) and deposition of distinct RNAs into platelets (Figure 6D-E) are unique in shedding light into the RNA dynamics during thrombopoiesis.

Posttranscriptional processes involved in MK gene regulation are poorly understood, although critical.[70,72,73] We show that SRSF3 is not essential for MK cell survival or endomitosis but controls a specific gene expression program vital for MK maturation and platelet release. Although in the control, MK RNAs encoding proteins with key MK and platelet functions were induced from 8N to ≥16N, in *Srsf3*-null MKs there was little difference between the 8N and ≥16N transcriptomes (Figure 5B-C). Comparisons of the dysregulated RNAs to our CLIP data in mouse pluripotent cells as well as experimental validation using an in vitro cell line model demonstrated that many functionally relevant MK RNAs were bound by SRSF3, thus placing SRSF3 as a direct regulator of MK RNA profile during maturation. Mechanistically, SRSF3 governed MK RNAs through processes it regulates in other cells types, such as nucleo-cytoplasmic mRNA export. As a nucleo-cytoplasmic mRNA export adaptor, SRSF3 depletion can cause a nuclear accumulation of its target RNAs.[28,64,65] In line with this, SRSF3 depletion compromised the export of key MK mRNAs encoding the cell surface receptors c-MPL and CD41. The nuclear accumulation of *Mpl* and *Itga2b* in SRSF3-depleted cells may explain the reduced level of c-MPL and CD41 in *Pf4-Srsf3*$^{\Delta/\Delta}$ MKs.

Because platelets are cytoplasmic fragments of MKs lacking genomic DNA, their RNA is produced by the parent cells. Recent studies have proposed an active sorting of functionally significant RNAs into platelets,[24,69-71] but no regulators of the sorting process are known. The abnormal RNA repertoire in platelets produced by *Srsf3*-null MKs suggests that SRSF3 could restrict and/or facilitate the deposition of distinct MK RNAs into platelets (Figure 6G) and thus serve as an mRNA adaptor also in the cytoplasm. Although the platelet RNA content reflected the MK RNA levels (supplemental Figure 6C), it was not a direct cross-section of MK RNAs as evidenced by the left-shift in platelet/MK RNA ratio distribution similar to previous observations (Figure 6C-D).[25] In *Pf4-Srsf3*$^{\Delta/\Delta}$ mice, the platelet/MK RNA ratio distribution was bimodal with a left-shift, further suggesting a failure in sorting distinct MK RNAs into platelets (Figure 6E). SRSF3 depletion in MKs led to a decrease in MK RNAs such as *Gp6* that aligned with a reduced level of *Gp6* mRNA in platelets (Figure 6F). The GPVI protein on platelet surface was also reduced, and purified *Pf4-Srsf3*$^{\Delta/\Delta}$ platelets displayed reduced response to GPVI

Figure 6 (continued) abundant in *Pf4-Srsf3*$^{\Delta/\Delta}$ platelets, and the points marked in red were more abundant when compared with control (FDR <0.05, FC >2). (C) Pearson correlation between DEGs during MK maturation (FDR <0.05, FC = 2) and platelet RNA levels. (D-E) Frequency distribution histograms of platelet/MK RNA abundance ratio (platelet CPM/MK ≥16N CPM) in control and *Pf4-Srsf3*$^{\Delta/\Delta}$. The dotted line marks 0. (F) Levels of RNAs encoding proteins central for platelet function in control and *Pf4-Srsf3*$^{\Delta/\Delta}$ 8N and ≥16N MKs and platelets. (G) A schematic depicting how SRSF3 governs a MK maturation program through RNA regulatory mechanisms such as mRNA export and guides the deposition of RNA into platelets. In the schematic, the black lines represent SRSF3 target RNAs in MKs, white lines, other MK RNAs and green balls are SRSF3. The data in panels A and F is presented as mean plus or minus SEM. Two-tailed unpaired Student *t* test; *$P \leq .05$. CPM; counts per million; PLT, platelet.

agonist (convulxin) stimulation (Figure 3A-B). Although the cytoplasmic *Mpl* and *Itga2b* mRNA levels were reduced in *Pf4-Srsf3*$^{\Delta/\Delta}$ MKs (Figure 5I; supplemental Figure 5M), the *Mpl* and *Itga2b* mRNA abundance in platelets was only moderately affected (Figure 6F). SRSF3 depletion in MKs led to reduced *Nbeal2* mRNA levels in MKs but increased levels in platelets, further exemplifying how not all MK RNAs are equal, and some MK RNAs are preferentially deposited into platelets. Because platelet RNAs are actively translated and degraded, and play a role in platelet responses to cellular cues,[20,21,68,71] determining how platelets get their RNA contributes to understanding of basic hemostasis and advances the knowledge of platelet response during cellular stress, infection, and disease.

The phenotype of the *Pf4-Srsf3*$^{\Delta/\Delta}$ mice resembles human macrothrombocytopenias (Table 2).[58] For example, we identified *Nbeal2*, causative of Gray platelet syndrome, as a direct SRSF3 RNA target.[74] *Nbeal2* was among the RNAs that were not properly induced from 8N to ≥16N MK following SRSF3 depletion. The *Pf4-Srsf3*$^{\Delta/\Delta}$ mice shared some features with *Nbeal2* loss-of-function models, including macrothrombocytopenia, reduction in platelet granule density, and increased emperipolesis associated with platelet pathologies and hematopoietic stress.[74-76] Thus, the *Pf4-Srsf3*$^{\Delta/\Delta}$ mouse model may provide a tool to understand platelet disorders, in particular the role of posttranscriptional gene regulation in platelet diseases. Albeit the SRSF3 depletion was limited to MKs, *Pf4-Srsf3*$^{\Delta/\Delta}$ mice displayed changes in peripheral blood and bone marrow hematopoietic cell counts, suggesting that the MK maturation defect in *Pf4-Srsf3*$^{\Delta/\Delta}$ mice may affect hematopoiesis more broadly in line with the previously identified functional relationship between MKs and hematopoietic stem cells.[77-79]

In conclusion, our study demonstrates how the RNA binding protein SRSF3 governs a MK maturation program that further guides the deposition of RNA into platelets, thus providing key insights into the role of posttranscriptional gene regulation during thrombopoiesis.

Acknowledgments

The authors thank Tyra Fraser, Marie Lee, Jessica Hatwell-Humble, and Daniela Cardozo for technical assistance; Benjamin Kile for helpful discussions on platelet biology; Richard Allcock for technical advice for platelet RNA sequencing; the support from MHTP Medical Genomics Platform in next-generation sequencing; and staff from FlowCore, Monash Histology Platform, and Monash Animal Research Platform (Monash University, Australia).

This work was supported by the Victorian Government Operational Infrastructure Support Scheme and Monash University Strategic Grant (M.-L.Ä.); a CSIRO OCE Science Leader Fellowship (S.K.N.); Independent Research Institutes Infrastructure Support Scheme Grant (9000220) from the Australian National Health and Medical Research Council (E.C.J.); a fellowship from the Lorenzo and Pamela Galli Charitable Trust; a Victorian State Government Operational Infrastructure Support Grant (E.C.J.); and a Gunn Family National Career Development Fellowship for Women in Haematology from the Snowdome Foundation and Maddie Riewoldt's Vision (B.B.G.). The Australian Regenerative Medicine Institute is supported by grants from the State Government of Victoria and the Australian Government. The funders had no part in the design, conduct, outcomes, decision to publish, or the drafting of this manuscript.

Authorship

Contribution: S.Y.H., S.K.N., and M.-L.Ä. designed the project; S.Y.H., T.A., B.B.G., P.G., E.C.J., S.L.E., M.R., H.C., B.C., C.K.H., B.W., J.F.W., M.F., M.R., S.K.N., and M.-L.Ä. performed the experiments; M.M., M.R., B.B.G., and M.-L.Ä., performed the bioinformatics analysis; S.Y.H., T.A., E.C.J., P.G., S.K.N., and M.-L.Ä. analyzed the data and made the figures; M.-L.Ä. wrote the manuscript; and all authors provided comments and approved the final manuscript.

Conflict-of-interest disclosure: The authors declare no competing financial interests.

ORCID profiles: T.A., 0000-0001-5910-2309; B.B.G., 0000-0003-2146-8561; E.C.J., 0000-0001-6478-5204; S.L.E., 0000-0002-5772-6051; M.R., 0000-0001-7252-1823; J.F.W., 0000-0002-4855-0170; M.R., 0000-0001-6315-4777; M-L.Ä., 0000-0003-0446-3566.

Correspondence: Minna-Liisa Änkö, Hudson Institute of Medical Research, 27-31 Wright Street Clayton, VIC 3168, Australia; e-mail: minni.anko@hudson.org.au.

Footnotes

Submitted 27 August 2021; accepted 6 November 2021; prepublished online on *Blood* First Edition 1 December 2021. DOI 10.1182/blood.2021013826.

*S.Y.H. and T.A. contributed equally to this study.

†S.K.N. and M.-L.Ä. are joint supervisors.

RNA-sequencing data are deposited in Gene Expression Omnibus at National Center for Biotechnology Information with accession number GSE155620. See also supplemental Methods.

Requests for data sharing may be submitted to Minna-Liisa Änkö (minni.anko@hudson.org.au)

The online version of this article contains a data supplement

The publication costs of this article were defrayed in part by page charge payment. Therefore, and solely to indicate this fact, this article is hereby marked "advertisement" in accordance with 18 USC section 1734.

REFERENCES

1. Italiano JE Jr. Unraveling mechanisms that control platelet production. *Semin Thromb Hemost.* 2013;39(1):15-24.
2. Bluteau D, Lordier L, Di Stefano A, et al. Regulation of megakaryocyte maturation and platelet formation. *J Thromb Haemost.* 2009;7(Suppl 1):227-234.
3. Machlus KR, Italiano JE Jr. The incredible journey: from megakaryocyte development to platelet formation. *J Cell Biol.* 2013;201(6):785-796.
4. Maclachlan A, Watson SP, Morgan NV. Inherited platelet disorders: insight from platelet genomics using next-generation sequencing. *Platelets.* 2017;28(1):14-19.
5. Nurden AT, Nurden P. Inherited disorders of platelet function: selected updates. *J Thromb Haemost.* 2015;13(Suppl 1):S2-S9.
6. Katsumura KR, Bresnick EH; GATA Factor Mechanisms Group. The GATA factor revolution in hematology. *Blood.* 2017;129(15):2092-2102.

7. Avellino R, Delwel R. Expression and regulation of C/EBPα in normal myelopoiesis and in malignant transformation. *Blood*. 2017;129(15):2083-2091.

8. Porcher C, Chagraoui H, Kristiansen MS. SCL/TAL1: a multifaceted regulator from blood development to disease. *Blood*. 2017; 129(15):2051-2060.

9. de Bruijn M, Dzierzak E. Runx transcription factors in the development and function of the definitive hematopoietic system. *Blood*. 2017;129(15):2061-2069.

10. Nürnberg ST, Rendon A, Smethurst PA, et al; HaemGen Consortium. A GWAS sequence variant for platelet volume marks an alternative DNM3 promoter in megakaryocytes near a MEIS1 binding site. *Blood*. 2012;120(24):4859-4868.

11. Chen L, Kostadima M, Martens JHA, et al. Transcriptional diversity during lineage commitment of human blood progenitors. *Science*. 2014;345(6204):1251033.

12. Pimentel H, Parra M, Gee SL, Mohandas N, Pachter L, Conboy JG. A dynamic intron retention program enriched in RNA processing genes regulates gene expression during terminal erythropoiesis. *Nucleic Acids Res*. 2016;44(2):838-851.

13. Wong JJ, Ritchie W, Ebner OA, et al. Orchestrated intron retention regulates normal granulocyte differentiation. *Cell*. 2013;154(3):583-595.

14. Cheng AW, Shi J, Wong P, et al. Muscleblind-like 1 (Mbnl1) regulates pre-mRNA alternative splicing during terminal erythropoiesis. *Blood*. 2014;124(4):598-610.

15. Edwards CR, Ritchie W, Wong JJ, et al. A dynamic intron retention program in the mammalian megakaryocyte and erythrocyte lineages. *Blood*. 2016;127(17):e24-e34.

16. Graubert TA, Shen D, Ding L, et al. Recurrent mutations in the U2AF1 splicing factor in myelodysplastic syndromes. *Nat Genet*. 2011;44(1):53-57.

17. Yoshida K, Sanada M, Shiraishi Y, et al. Frequent pathway mutations of splicing machinery in myelodysplasia. *Nature*. 2011; 478(7367):64-69.

18. Qiu J, Zhou B, Thol F, et al. Distinct splicing signatures affect converged pathways in myelodysplastic syndrome patients carrying mutations in different splicing regulators. *RNA*. 2016;22(10):1535-1549.

19. Albers CA, Paul DS, Schulze H, et al. Compound inheritance of a low-frequency regulatory SNP and a rare null mutation in exon-junction complex subunit RBM8A causes TAR syndrome. *Nat Genet*. 2012; 44(4):435-439.

20. Mills EW, Wangen J, Green R, Ingolia NT. Dynamic regulation of a ribosome rescue pathway in erythroid cells and platelets. *Cell Rep*. 2016;17(1):1-10.

21. Denis MM, Tolley ND, Bunting M, et al. Escaping the nuclear confines: signal-dependent pre-mRNA splicing in anucleate platelets. *Cell*. 2005;122(3):379-391.

22. Rowley JW, Oler AJ, Tolley ND, et al. Genome-wide RNA-seq analysis of human and mouse platelet transcriptomes [published correction appears in *Blood*. 2014;123(24):3843]. *Blood*. 2011;118(14): e101-e111.

23. Schubert S, Weyrich AS, Rowley JW. A tour through the transcriptional landscape of platelets. *Blood*. 2014;124(4):493-502.

24. Cecchetti L, Tolley ND, Michetti N, Bury L, Weyrich AS, Gresele P. Megakaryocytes differentially sort mRNAs for matrix metalloproteinases and their inhibitors into platelets: a mechanism for regulating synthetic events. *Blood*. 2011;118(7): 1903-1911.

25. Mills EW, Green R, Ingolia NT. Slowed decay of mRNAs enhances platelet specific translation. *Blood*. 2017;129(17):e38-e48.

26. Zhong X-Y, Wang P, Han J, Rosenfeld MG, Fu X-D. SR proteins in vertical integration of gene expression from transcription to RNA processing to translation. *Mol Cell*. 2009; 35(1):1-10.

27. Änkö M-L. Regulation of gene expression programmes by serine-arginine rich splicing factors. *Semin Cell Dev Biol*. 2014;32:11-21.

28. Huang Y, Steitz JA. Splicing factors SRp20 and 9G8 promote the nucleocytoplasmic export of mRNA. *Mol Cell*. 2001;7(4): 899-905.

29. Cavaloc Y, Bourgeois CF, Kister L, Stévenin J. The splicing factors 9G8 and SRp20 transactivate splicing through different and specific enhancers. *RNA*. 1999;5(3):468-483.

30. Lou H, Neugebauer KM, Gagel RF, Berget SM. Regulation of alternative polyadenylation by U1 snRNPs and SRp20. *Mol Cell Biol*. 1998;18(9):4977-4985.

31. Auyeung VC, Ulitsky I, McGeary SE, Bartel DP. Beyond secondary structure: primary-sequence determinants license pri-miRNA hairpins for processing. *Cell*. 2013;152(4): 844-858.

32. Änkö M-L, Müller-McNicoll M, Brandl H, et al. The RNA-binding landscapes of two SR proteins reveal unique functions and binding to diverse RNA classes. *Genome Biol*. 2012; 13(3):R17.

33. Ratnadiwakara M, Archer SK, Dent CI, et al. SRSF3 promotes pluripotency through *Nanog* mRNA export and coordination of the pluripotency gene expression program. *eLife*. 2018;7:e37419.

34. Änkö M-L, Morales L, Henry I, Beyer A, Neugebauer KM. Global analysis reveals SRp20- and SRp75-specific mRNPs in cycling and neural cells. *Nat Struct Mol Biol*. 2010; 17(8):962-970.

35. Jumaa H, Wei G, Nielsen PJ. Blastocyst formation is blocked in mouse embryos lacking the splicing factor SRp20. *Curr Biol*. 1999;9(16):899-902.

36. Ohta S, Nishida E, Yamanaka S, Yamamoto T. Global splicing pattern reversion during somatic cell reprogramming. *Cell Rep*. 2013; 5(2):357-366.

37. Sen S, Jumaa H, Webster NJ. Splicing factor SRSF3 is crucial for hepatocyte differentiation and metabolic function. *Nat Commun*. 2013;4(1):1336.

38. Hobeika E, Thiemann S, Storch B, et al. Testing gene function early in the B cell lineage in mb1-cre mice. *Proc Natl Acad Sci USA*. 2006;103(37):13789-13794.

39. Jumaa H, Guénet JL, Nielsen PJ. Regulated expression and RNA processing of transcripts from the Srp20 splicing factor gene during the cell cycle. *Mol Cell Biol*. 1997;17(6):3116-3124.

40. Jia R, Li C, McCoy JP, Deng CX, Zheng ZM. SRp20 is a proto-oncogene critical for cell proliferation and tumor induction and maintenance. *Int J Biol Sci*. 2010;6(7):806-826.

41. He X, Arslan AD, Pool MD, et al. Knockdown of splicing factor SRp20 causes apoptosis in ovarian cancer cells and its expression is associated with malignancy of epithelial ovarian cancer. *Oncogene*. 2011;30(3): 356-365.

42. Tiedt R, Schomber T, Hao-Shen H, Skoda RC. Pf4-Cre transgenic mice allow the generation of lineage-restricted gene knockouts for studying megakaryocyte and platelet function in vivo. *Blood*. 2007;109(4): 1503-1506.

43. Dobin A, Davis CA, Schlesinger F, et al. STAR: ultrafast universal RNA-seq aligner. *Bioinformatics*. 2013;29(1):15-21.

44. McCarthy DJ, Chen Y, Smyth GK. Differential expression analysis of multifactor RNA-Seq experiments with respect to biological variation. *Nucleic Acids Res*. 2012; 40(10):4288-4297.

45. Robinson MD, McCarthy DJ, Smyth GK. edgeR: a Bioconductor package for differential expression analysis of digital gene expression data. *Bioinformatics*. 2010; 26(1):139-140.

46. Guo BB, Linden MD, Fuller KA, et al. Platelets in myeloproliferative neoplasms have a distinct transcript signature in the presence of marrow fibrosis. *Br J Haematol*. 2020;188(2):272-282.

47. Love MI, Huber W, Anders S. Moderated estimation of fold change and dispersion for RNA-seq data with DESeq2. *Genome Biol*. 2014;15(12):550.

48. Huang W, Sherman BT, Lempicki RA. Systematic and integrative analysis of large gene lists using DAVID bioinformatics resources. *Nat Protoc*. 2009;4(1):44-57.

49. Aubrey BJ, Kelly GL, Kueh AJ, et al. An inducible lentiviral guide RNA platform enables the identification of tumor-essential genes and tumor-promoting mutations in vivo. *Cell Rep*. 2015;10(8):1422-1432.

50. Jumaa H, Nielsen PJ. The splicing factor SRp20 modifies splicing of its own mRNA and ASF/SF2 antagonizes this regulation. *EMBO J*. 1997;16(16):5077-5085.

51. Levine RF, Hazzard KC, Lamberg JD. The significance of megakaryocyte size. *Blood*. 1982;60(5):1122-1131.

52. Raslova H, Kauffmann A, Sekkaï D, et al. Interrelation between polyploidization and megakaryocyte differentiation: a gene profiling approach. *Blood*. 2007;109(8): 3225-3234.

53. Larson MK, Watson SP. Regulation of proplatelet formation and platelet release by integrin alpha IIb beta3. *Blood*. 2006;108(5): 1509-1514.

54. Ng AP, Kauppi M, Metcalf D, et al. Mpl expression on megakaryocytes and platelets is dispensable for thrombopoiesis but essential to prevent myeloproliferation. *Proc Natl Acad Sci USA*. 2014;111(16):5884-5889.

55. Ebbe S, Stohlman F Jr. Megakaryocytopoiesis in the rat. *Blood*. 1965;26(1):20-35.

56. Hartwig J, Italiano J Jr. The birth of the platelet. *J Thromb Haemost*. 2003;1(7): 1580-1586.

57. Nurden AT, Nurden P. The gray platelet syndrome: clinical spectrum of the disease. *Blood Rev*. 2007;21(1):21-36.

58. Favier R, Raslova H. Progress in understanding the diagnosis and molecular genetics of macrothrombocytopenias. *Br J Haematol*. 2015;170(5):626-639.

59. Balduini CL, Savoia A. Genetics of familial forms of thrombocytopenia. *Hum Genet*. 2012;131(12):1821-1832.

60. Ault KA, Knowles C. In vivo biotinylation demonstrates that reticulated platelets are the youngest platelets in circulation. *Exp Hematol*. 1995;23(9):996-1001.

61. Deppermann C, Cherpokova D, Nurden P, et al. Gray platelet syndrome and defective thrombo-inflammation in Nbeal2-deficient mice. *J Clin Invest*. 2013;123(8):3331-3342.

62. Kahr WH, Lo RW, Li L, et al. Abnormal megakaryocyte development and platelet function in Nbeal2(-/-) mice. *Blood*. 2013; 122(19):3349-3358.

63. Fletcher SJ, Johnson B, Lowe GC, et al; UK Genotyping and Phenotyping of Platelets study group. SLFN14 mutations underlie thrombocytopenia with excessive bleeding and platelet secretion defects. *J Clin Invest*. 2015;125(9):3600-3605.

64. Huang Y, Gattoni R, Stévenin J, Steitz JA. SR splicing factors serve as adapter proteins for TAP-dependent mRNA export. *Mol Cell*. 2003;11(3):837-843.

65. Müller-McNicoll M, Botti V, de Jesus Domingues AM, et al. SR proteins are NXF1 adaptors that link alternative RNA processing to mRNA export. *Genes Dev*. 2016;30(5):553-566.

66. Gnatenko DV, Dunn JJ, McCorkle SR, Weissmann D, Perrotta PL, Bahou WF. Transcript profiling of human platelets using microarray and serial analysis of gene expression. *Blood*. 2003;101(6):2285-2293.

67. Bugert P, Dugrillon A, Günaydin A, Eichler H, Klüter H. Messenger RNA profiling of human platelets by microarray hybridization. *Thromb Haemost*. 2003;90(4):738-748.

68. Weyrich AS, Dixon DA, Pabla R, et al. Signal-dependent translation of a regulatory protein, Bcl-3, in activated human platelets. *Proc Natl Acad Sci USA*. 1998;95(10):5556-5561.

69. Preußer C, Hung LH, Schneider T, et al. Selective release of circRNAs in platelet-derived extracellular vesicles. *J Extracell Vesicles*. 2018;7(1):1424473.

70. Fisher MH, Di Paola J. Genomics and transcriptomics of megakaryocytes and platelets: implications for health and disease. *Res Pract Thromb Haemost*. 2018; 2(4):630-639.

71. Rowley JW, Schwertz H, Weyrich AS. Platelet mRNA: the meaning behind the message. *Curr Opin Hematol*. 2012;19(5):385-391.

72. Landry P, Plante I, Ouellet DL, Perron MP, Rousseau G, Provost P. Existence of a microRNA pathway in anucleate platelets. *Nat Struct Mol Biol*. 2009;16(9):961-966.

73. Rowley JW, Chappaz S, Corduan A, et al. Dicer1-mediated miRNA processing shapes the mRNA profile and function of murine platelets. *Blood*. 2016;127(14): 1743-1751.

74. Kahr WH, Hinckley J, Li L, et al. Mutations in NBEAL2, encoding a BEACH protein, cause gray platelet syndrome. *Nat Genet*. 2011; 43(8):738-740.

75. Cunin P, Nigrovic PA. Megakaryocyte emperipolesis: a new frontier in cell-in-cell interaction. *Platelets*. 2020;31(6): 700-706.

76. Di Buduo CA, Alberelli MA, Glembostky AC, et al. Abnormal proplatelet formation and emperipolesis in cultured human megakaryocytes from gray platelet syndrome patients [published correction appears in *Sci Rep*. 2016;6:25027]. *Sci Rep*. 2016;6(1):23213.

77. Heazlewood SY, Neaves RJ, Williams B, Haylock DN, Adams TE, Nilsson SK. Megakaryocytes co-localise with hemopoietic stem cells and release cytokines that up-regulate stem cell proliferation. *Stem Cell Res (Amst)*. 2013;11(2):782-792.

78. Bruns I, Lucas D, Pinho S, et al. Megakaryocytes regulate hematopoietic stem cell quiescence through CXCL4 secretion. *Nat Med*. 2014;20(11):1315-1320.

79. Zhao M, Perry JM, Marshall H, et al. Megakaryocytes maintain homeostatic quiescence and promote post-injury regeneration of hematopoietic stem cells. *Nat Med*. 2014;20(11):1321-1326.